Materials Science-Poland, 32(4), 2014, pp. 633-640
http://www.materialsscience.pwr.wroc.pl/
DOI: 10.2478/s13536-014-0240-y

VERSITA

Magnetic properties of manganese doped $PrAlO_3$ monocrystalline fibres

A. GUZIK[1]*, E. TALIK[1], A. PAJĄCZKOWSKA[2], S. TURCZYŃSKI[2], J. KUSZ[1]

[1]A. Chelkowski Institute of Physics, Silesian University, Uniwersytecka 4, 40-007 Katowice, Poland
[2]Institute of Electronics Materials Technology, Wolczynska 133, 01-919 Warsaw, Poland

Monocrystalline fibres of undoped $PrAlO_3$ and $PrAlO_3$:0.1 Mn, have been grown by the pulling-down method under nitrogen atmosphere. The as-grown crystal doped with Mn had a visible brown core surrounded by a green ring, whereas this effect was weaker for the undoped $PrAlO_3$. A coloration of the brown core was caused by a presence of Pr^{4+} ions. The presence of the Pr^{4+} ions was confirmed by XPS and magnetic studies. The XPS chemical analysis showed the increased concentration of oxygen in the crystals with the brown core. The most probable valency of manganese is Mn^{4+}. It is located in Al^{3+} sites.

Keywords: *oxides; crystal growth; electronic structure; magnetic property*

1. Introduction

$PrAlO_3$ belongs to a wide group of compounds called perovskites. As in many others, its crystal structure is unstable with temperature and several crystallographic transitions occur. Below the melting point at 2350 K [1] the compound crystallizes in a cubic structure, space group (S.G.) Pm-3m. Below 1864 K [1, 2] or 1650 K [3], depending on literature, the structure is transformed into a rhombohedral one with S.G. R-3c. Lowering the temperature below 220 K leads to transformations of the structure into orthorhombic (S.G. Imma), and finally below 155 K, into monoclinic, S.G. C2/m [2–7]. The structural changes are reflected in the magnetic properties. In the rhombohedral phase (1650 to 220 K), susceptibility follows the Curie-Weiss law. The effective magnetic moment of 3.48 μ_B and the Curie-Weiss temperature of 14 K have been reported [8]. A very large magnetic effective moment, equal to 4.86 μ_B with a very large negative Curie-Weiss temperature of 103 K, has been found in the orthorhombic phase (220 to 155 K) [8]. In the monoclinic phase (below 155 K) the magnetic susceptibility shows a Van Vleck paramagnetism [9]. At low temperatures it becomes temperature-independent according to results of Wencka et al. [9]. In the crystal electric field, the $4f^2$ multiplet of Pr^{3+} ($^3H_4$) splits into a singlet, a doublet and two triplets, though a singlet is usually the ground state. At low temperatures, only the ground singlet is populated, leading to the temperature independent susceptibility [10].

The single crystal of the $PrAlO_3$ compound has been grown by the Czochralski method [8, 10] and its electronic structure was investigated [11]. It was shown that the as-grown crystal had a brown colour, similar to that of the mixed valence praseodymium oxide, Pr_6O_{11}. After annealing under H_2/N_2 atmosphere, the brown colour changed to green, characteristic of Pr^{3+} admixtures. Such changes in optical properties, supported by X-ray photoelectron spectroscopy (XPS) measurements, have been explained by removing an excess of oxygen from the sample and successive transformation of Pr^{4+} into Pr^{3+} ions in order to keep charge neutrality. Even after a thermal treatment, the crystal had a composition of $Pr_{0.9}Al_{0.9}O_{3.09}$, showing a presence of interstitial oxygen.

As far as we know, one report concerning the growth of the $PrAlO_3$ doped with Ce and Sr by

*E-mail: adam.guzik@us.edu.pl

the pulling-down method has been published so far [12]. For the undoped $PrAlO_3$ grown by the Czochralski method, a potential application could be a tunable laser in the whole visible region. Unfortunately, at this stage, the emission seems rather weak [10].

Recently, it has been observed that $YAlO_3$ (YAP) doped with manganese exhibits efficient thermoluminescence. For the concentration of Mn ions of about 0.05 at.%, YAP is a very good detector of the gamma radiation and it makes possible to measure doses from about 10^{-2} Gy up to about 10 kGy. The strongest thermoluminescence is observed for Mn^{2+}. The Mn^{2+} ions in this perovskite are active fluorescent centers responsible for yellow-green thermoemission with a maximum near 530 nm [13, 14]. Therefore, it is a material suitable for the thermoluminescent dosimeter, which can find the use in medical and biological technologies. The aim of this work was to obtain and characterize the crystals: undoped $PrAlO_3$ and $PrAlO_3$ doped with manganese of the nominal composition $PrAlO_3$:0.1Mn, grown by the pulling-down method, as a potential optoelectronic material.

2. Experimental

The melts were prepared from high purity oxides: Pr_6O_{11} (99.995 %), Al_2O_3 (99.999 % Testbourne Ltd.), MnO (99.99 % Alfa Aesar). First, the oxide powders were dried at 350 °C for 4 h. Then they were mixed in a mechanical stirrer in stoichiometric ratios to obtain composition $PrAlO_3$:0.1Mn. Afterwards, the powders were grinded in an agate mortar. Finally, the raw materials were annealed at 1100 °C for 6 h.

The $PrAlO_3$ crystalline fibres were grown using a micro-pulling-down method (μ-PD). The μ-PD method was invented in Japan, originally for the growth of single crystal fibres [15–18]. The melt passes through a nozzle in an iridium crucible, and then it comes into contact with the "seed": in our case iridium wire, and the crystal is then pulled down. The fibres were grown at a pulling rate of 0.05 mm/min in the form of rods ∼3 mm in diameter and few centimetres in length. A nitrogen atmosphere was applied.

The X-ray measurement data were collected using the single crystal Xcalibur Kappa diffractometer (Oxford Diffraction) with a Sapphire3 CCD detector. The crystals with a size of ∼0.15 mm were mounted on a glass capillary and measured at 280 K. Accurate cell parameters were determined from about 1500 strong Bragg reflections and refined using the program CrysAlis CCD. In the diffraction image no powder rings (Fig. 1c) were observed.

The XPS spectra were obtained using the PHI 5700/660 Physical Electronics Photoelectron Spectrometer with monochromatized Al Kα X-ray radiation (1486.6 eV). The hemispherical mirror analyzer measured the energy of the electrons with a resolution of about 0.3 eV. The photoelectron emission from a surface area of 800 μm × 800 μm was recorded. The crystals were broken and measured under UHV conditions of an order of 10^{-8} Pa. In every case a neutralizer was used because of a charge effect, which occurred for non-conducting samples. The binding energy was determined with reference to the C 1s line at 284.8 eV of adventitious carbon. The Gaussian-Lorenzian functions were used to fit the XPS core level spectra.

Magnetic properties were investigated with the Quantum Design MPMS XL7 magnetometer. Magnetic susceptibilities were measured under magnetic field of 1 T in the temperature range of 2 to 400 K. Samples were cooled under magnetic field of 1 T. Magnetic isotherms were measured in magnetic field up to 7 T.

The SEM/EDS method using the X-max detector by Oxford Instruments, being an equipment of the JEOL JSM 7600 F scanning electron microscope, was used. It was based on 20 mm^2 Silicon Drift Detector calibrated using the Mn Kα line giving the line width (resolution) of 125 eV.

3. Results and discussion

The cross-sections perpendicular to the growth direction of two single crystals: the undoped $PrAlO_3$ and the $PrAlO_3$ doped nominally with

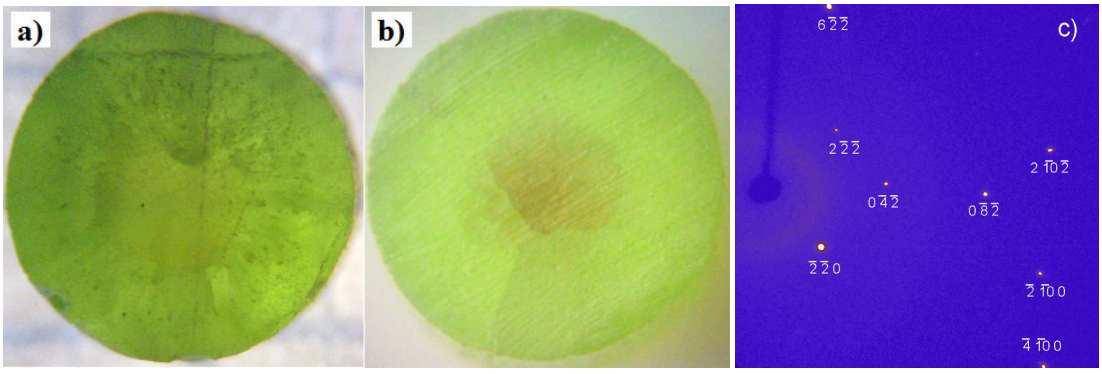

Fig. 1. Optical microscope images (× 50) of the cross-sections of undoped (a) and Mn doped (b) single crystals; the rods diameter is about 3 mm; squares visible beyond the crystal come from a plotting paper. The surface after cutting has not been polished, so it is not opaque. The diffraction image of the undoped crystal is shown in (c).

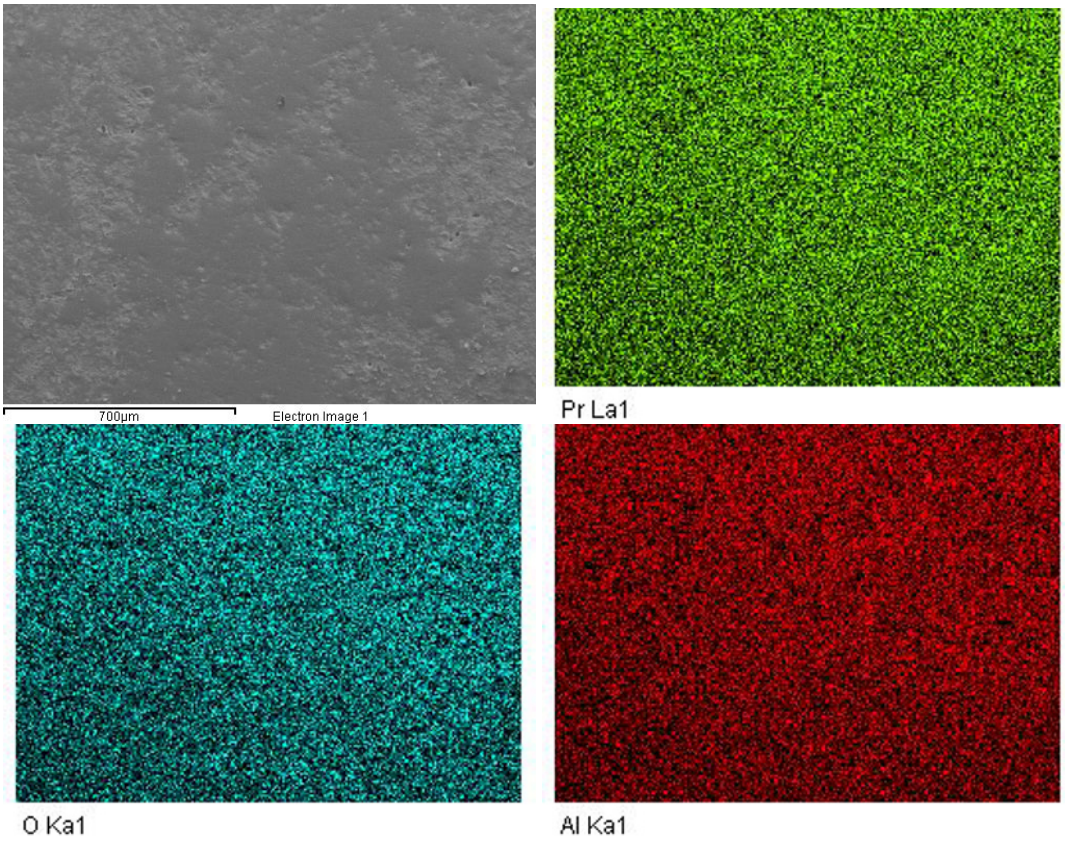

Fig. 2. SEM image and its corresponding EDS profile of a doped sample. The bar below the electron image represents 700 µm.

0.1 Mn are shown in Fig. 1a and 1b, respectively. Both crystals have a clearly visible core. In the undoped crystal the core has a brownish-green colour, whereas the core of the doped sample is brown and the ring of the sample is green. The outer part of the undoped sample has many defects aligned radially, while for the doped sample, besides of the core, the brownish growth zone seems to exist. Such defects

can make ways for diffusion of contaminants, e.g carbon and oxygen, into the sample. The SEM image and its corresponding elemental analysis with EDS profile of the core area of the doped sample is presented in Fig. 2. Two-dimensional (2D) elemental mapping of Pr, Al, and O demonstrates that all three elements have been homogeneously distributed across the crystal.

The wide range XPS spectrum of the doped crystal is shown in Fig. 3. It shows the core elements and a prominent amount of carbon. The carbon presence can be attributed to the defects visible on the slice photograph (Fig. 1b). In other single crystals, e.g. $GdCa_4O(BO_3)_3$, the presence of carbon inside a transparent colourless single crystal has been explained via detailed X-ray topography investigations. It has been found that carbon migrated into the single crystal via radially distributed dislocations [19].

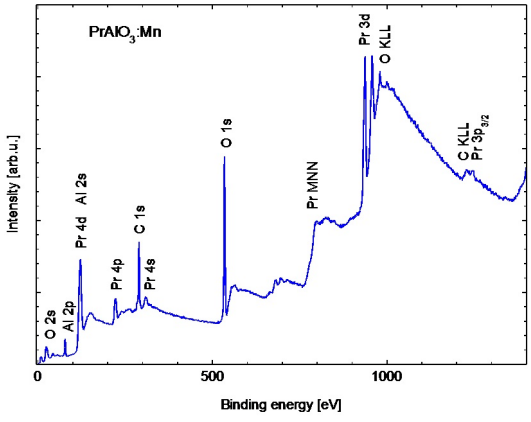

Fig. 3. XPS spectrum of the doped sample in the wide energy range. Besides the core lines (e.g. Pr3d) Auger electrons are visible (e.g. C KLL).

The calculated chemical composition, determined by the XPS method, is $Pr_{0.90}Al_{0.96}O_{3.14}Mn_{0.02}$. Another method to estimate the composition is the energy dispersive spectrophotometry (EDS). The composition estimated by this way is $Pr_{0.92\pm0.06}Al_{0.90\pm0.002}O_{3.18\pm0.02}$. Manganese has not been detected by the EDS because the characteristic X-ray lines from Pr and Mn differ slightly and overlap. The composition of the undoped crystal estimated by EDS method is $Pr_{0.94\pm0.06}Al_{1\pm0.003}O_{3.06\pm0.02}$. In both methods, elemental identification is detectable for the spectra of good quality within a limit of 0.1 at.%. However, having some experience and a good instrument we were able to include the second decimal place as an indicative (not certain) value. Therefore, the increase in the oxygen content with Mn doping is observed.

The lattice parameters are collected in Table 1 and compared with the literature data. The lattice parameter a of the doped sample is slightly smaller than that in the undoped one. Taking into account that the radius of Pr^{3+} in the dodecahedral coordination is 1.33 Å [20], radius of Pr^{4+} is unknown but should be smaller and the radiuses of octahedral Mn^{4+}, Mn^{3+} LS, Mn^{3+} HS and Al^{3+} are 0.53 Å, 0.58 Å, 0.65 Å, 0.675 Å, respectively, we can conclude that for the doped sample the non-significant decrease of the lattice parameter may be caused by both contributions: manganese and/or Pr^{4+}.

Table 1. Lattice parameters for undoped and doped $PrAlO_3$ at room temperature (rhombohedral notation).

	a [Å]	α [deg]	
$PrAlO_3$ crystal a	5.309	60.24	[8]
crystal b	5.313	59.91	
$PrAlO_3$	5.3083	60.31	[10]
$PrAlO_3$	5.3259(2)	60.14(4)	this work
$PrAlO_3$: $Mn_{0.02}$ core	5.3249(1)	60.17(6)	this work
$PrAlO_3$: $Mn_{0.02}$ ring	5.3250(5)	60.17(1)	

Because the position of the XPS Al2p line (Fig. 4a) in the doped sample changes due to the chemical shift (Table 2), we can expect that the manganese ions occupy the aluminium positions. Taking into account the decrease of the lattice parameter in the doped sample, the Mn^{3+} LS or Mn^{4+} configuration seems to be the most suitable.

As revealed by the thermoluminescence studies, manganese ions in these compounds are observed mainly due to the presence of Mn^{4+} in Al position. These samples are also characterized by a very low efficiency of thermoluminescence of manganese ions [21].

The Al2p, O1s and Pr3d XPS lines, visible in Fis. 4a, 4b and Fig. 5, have been deconvoluted

Table 2. Binding energies of Pr3d, Al2p, O1s for undoped and doped $PrAlO_3$.

Sample	$Pr3d_{5/2}$ (931.8 eV)*	Al2p (72.9 eV)*	O1s (531 eV)*
$PrAlO_3$ [11]	932.3 $\Delta = 0.5$ eV	73.0 $\Delta = 0.1$ eV	529.3 $\Delta = -1.7$ eV
$PrAlO_3$: $Mn_{0.02}$ this work	932.3 $\Delta = 0.5$ eV	73.3 $\Delta = 0.4$ eV	529.5 $\Delta = -1.5$ eV

*Catalogue [21], Δ chemical shift

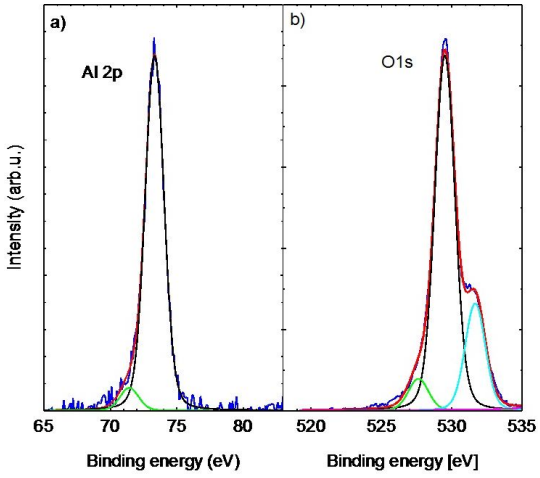

Fig. 4. XPS Al2p and O1s lines of the doped crystal.

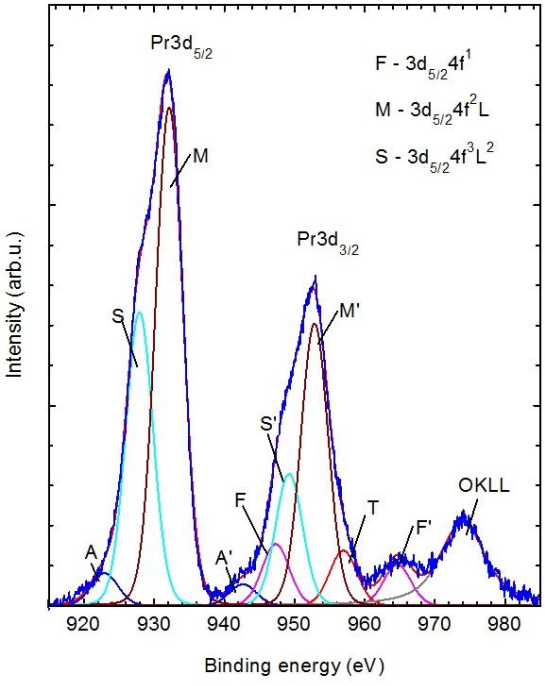

Fig. 5. XPS Pr3d lines of the doped crystal.

after background subtraction for the doped crystal. The binding energies of the observed states differ from those of the catalogue ones, and the states of $Pr3d_{5/2}$ are located at 932.3 eV (binding energy 0.5 eV stronger than in pure Pr), Al2p: 73.3 eV (+0.4 eV) and O1s: 529.5 eV (−1.5 eV). This indicates the presence of the mixed covalent and ionic bonds in the compound. The comparison of the binding energies of the undoped and doped $PrAlO_3$ is given in Table 2 [22]. The monocrystalline compound cited in the Table 2 was obtained by the Czochralski method [11]. The XPS binding energies of the Pr3d are almost the same for both samples, while the changes in binding energies for the Al2p and O1s are observed and may be related to the presence of Mn in the Al positions.

A deconvolution of the O1s line shows, except the main line, two additional lines: the first one at lower and the second one at higher binding energies. The main line is attributed to the constitutional oxygen. The higher energy line can be attributed to the external oxygen contamination and/or to the interstitial oxygen ions due to increased amount of it. For the lines Al2p, O1s and Pr3d low binding energy line are visible. These extra lines can be related to defects of the crystal structure.

The shape of the Pr3d lines (Fig. 5) of $PrAlO_3$ can be compared to that observed for Pr_2O_3 [11]. The complex shape originates from the simultaneous effect of solid state hybridization and intra-atomic electrostatic coupling between 3d hole and outer unpaired 4f electrons [23]. The $Pr3d_{3/2}$ and $3d_{5/2}$ lines are split due to final state configurations of $4f^3L^2$ (L-hole on the O2p valence band) on the low binding energy side (peaks S) and of the $4f^2L$ on the high energy side (peaks M) [23]. The $Pr3d_{3/2}$ has an additional peak on the tail of the main line on the high binding energy side (peak T), which can be also attributed to

a shake-up process. The doublet Pr3d at about 947.3 eV and 964.6 eV (peaks F) may be attributed to the $4f^1$ final state [23, 24], which can indicate the presence of Pr^{4+} ions. Intensity of the Pr^{4+} peak is ~6 % of the total intensity.

Magnetic susceptibilities of both samples were measured under magnetic field of 1 T (Fig. 6). Their temperature runs reflect the crystal structure transitions. The undoped crystal, in rhombohedral phase, has the effective magnetic moment equal to $\mu_{eff} = 3.60\ \mu_B$, the Curie-Weiss temperature $\theta = -54$ K and the temperature independent contribution $\chi_0 = -2.7{\cdot}10^{-5}$ emu/mol; in orthorhombic phase $\mu_{eff} = 3.99\ \mu_B$, $\theta = -77$ K and $\chi_0 = -5.24{\cdot}10^{-4}$ emu/mol. The theoretical, calculated from the Hunds rules, effective magnetic moment of the Pr^{3+} is equal to 3.58 μ_B. It means that only in the undoped crystal there are the Pr^{3+} ions, and there is a lack of the Pr^{4+} ions, which is consistent with the green colour of the sample.

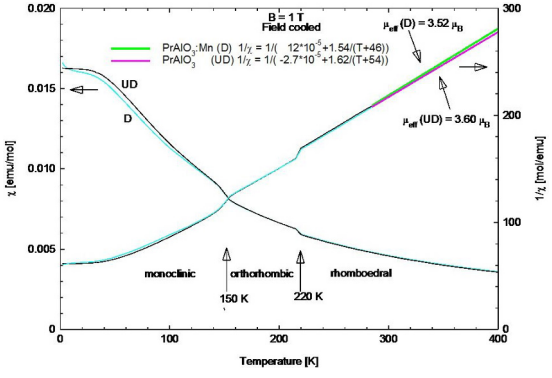

Fig. 6. The magnetic susceptibility of undoped and doped crystals. Fits to the modified Curie-Weiss law in the rhombohedral phase and estimated effective magnetic moments are also shown.

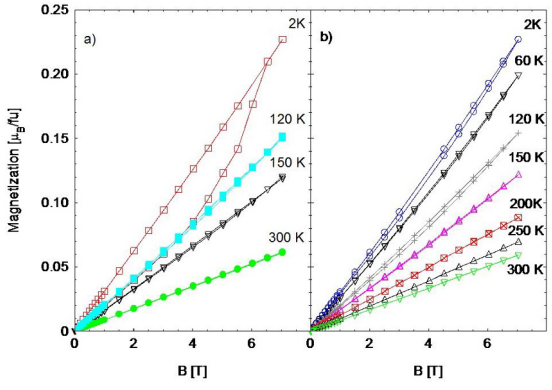

Fig. 7. Magnetic isotherms of the undoped (a) and doped sample (b). Hystereses are visble in monoclinic phase (at temperature below 155 K).

In the orthorhombic phase the enhanced effective magnetic moment can be attributed to the formation of the short range interaction areas. In the monoclinic phase, the susceptibility increases with lowering temperature. At a temperature range below 80 K the susceptibility seems to be a temperature independent. Such a run can be explained in terms of the Crystal Electric Field (CEF). The lowest CEF level of Pr^{3+} is usually a singlet. At low temperatures, the contribution to susceptibility is due to a second order induced magnetization, attributed to the Van Vleck temperature independent susceptibility. However, magnetization isotherms (Fig. 7a) show hysteresis in that phase. They are concave in an initial run but return and every next run gives a straight line. The magnetization is very far from saturation, as that observed under the magnetic field of 7 T is equal to 0.23 μ_B for the Pr ion at 2 K, whereas the theoretical saturation magnetization for Pr^{3+} is equal to 3.2 μ_B. The hystereses exist in the whole temperature range up to 150 K. Such peculiarities can be explained by the existence of the short range magnetic correlation areas. These areas are formed in the orthorhombic phase and they increase the magnetic susceptibility in that phase. They survive the crystallographic transformation keeping orthorhombic symmetry even in the monoclinic phase. Magnetic field rotates these areas, trying to align them along the magnetic field. It could cause a pseudo-metamagnetic behaviour.

The doped crystal in the rhombohedral and orthorhombic phases has similar magnetic properties to the undoped one (Fig. 6). In the rhombohedral structure the effective magnetic moment is equal to 3.52 μ_B, $\theta = -46$ K and $\chi_0 = 1.2{\cdot}10^{-4}$ emu/mol (Fig. 6), whereas in the orthorhombic phase the $\mu_{eff} = 3.83\ \mu_B$ and $\theta = -69$ K and $\chi_0 = -1.45{\cdot}10^{-4}$ emu/mol. The Van Vleck behaviour is observed in the temperature range of 15 to 80 K; below 15 K the

Curie-like dependence is reinforced. Magnetic isotherms (Fig. 7b) show the hysteresis in the whole temperature range of the monoclinic phase, however, not such spectacular. Therefore, in the doped crystal the short range correlations areas are aligned much easier than in the undoped one. The location of the Mn^{4+} ions with a magnetic moment in the Al sites may modify the short range correlations, which could result in the narrower hystereses.

The Pr^{4+} ions behave like Ce^{3+} ions, i.e. the ground state is a doublet, which can explain the Curie upturn at the lowest temperatures. The presence of the Pr^{4+} should decrease the effective magnetic moment in the sample because the theoretical μ_{eff} (Pr^{4+}), equal to 2.54 μ_B, is less than 3.2 μ_B for Pr^{3+}. From the XPS measurement, the contribution of the Pr^{4+} ions has been estimated as $\sim$6 %. Thus, the average effective magnetic moment for two different Pr ions should be equal to $\mu_{eff} = 3.526\ \mu_B$, close to the observed value of 3.52 μ_B. Due to the very small amount of manganese ions $\sim$2 %, no long range order is observed at higher temperatures. As the magnetic moment of Mn in isolators strongly depends on the ionic state (Mn^{4+}, Mn^{3+}) and a local symmetry, it is impossible to estimate its contribution. The attempt to estimate the valency of the Mn ions by the Electron Spin Resonance method failed due to overlapping signals from the Pr^{3+} ions and Mn. Therefore, the origin of the upturn (Pr^{4+}, Mn) in the magnetic susceptibility at the lowest temperature remains unclear and further investigations are necessary.

4. Conclusions

An investigation of the composition of $PrAlO_3$ crystal doped by Mn ions, using the XPS and EDS techniques gave consistent results. The excess of oxygen ions in the $PrAlO_3$ crystal structure caused stronger charge transfer at praseodymium ions in order to keep the charge neutrality, what resulted in the occurrence of the Pr^{4+} ions. It manifested visually as a brown core of the crystal. The XPS spectrum of the Pr 3d showed the contribution of $\sim$6 % attributed to the Pr^{4+} ions. The most probable valency of manganese is Mn^{4+} in Al sites. The presence of Pr^{4+} ions was confirmed also by the lowered magnetic effective moment in the doped sample. Therefore, the coloration, electronic structure and magnetic properties clearly indicate the presence of the Pr^{4+} ions in the doped sample.

Acknowledgements

This work was partially financed by the Polish National Science Centre under Grant No. NN 515 500 440. SQUID magnetometer was financed by European Regional Development Fund, whereas SEM/EDS JEOL was financed by Regional Fund for Environmental Protection and Water Management in Katowice.

References

[1] BASYUK T., VASYLECHKO L., FADEEV S., SYVOROTKA I.I., TROTS D., NIEWA R., *Radiat. Phys. Chem.*, 78 (2009), S97.
[2] CARPENTER M.A., HOWARD C.J., KENNEDY B.J., KNIGHT K.S., *Phys. Rev. B*, 72 (2005), 024118.
[3] MOUSSA S., KENNEDY B., HUNTER B., HOWARD C., VOGT T., *J. Phys.-Condens. Mat.*, 13 (2001), L203.
[4] HOWARD C.J., STOKES H., *Acta Crystallogr. B*, 54/6 (1998), 782.
[5] HOWARD C.J., KENNEDY B.J., CHAKOUMAKOS B.C., *J. Phys.-Condens. Mat.*, 12 (4) (2000), 349.
[6] KENNEDY B.J., PRODJOSANTOSO A.K., HOWARD C.J., *J. Phys.-Condens Mat.*, 11 (33) (1999), 6319.
[7] KENNEDY B.J., VOGT T., MARTIN C.D., PARISE J.B., HRIJAC J.A., *Chem. Mater.*, 14 (6) (2002), 2644.
[8] TURCZYNSKI S., ORLINSKI K., PAWLAK D.A., DIDUSZKO R., MUCHA J., PEKALA M., FAGNARD J., VANDERBEMDEN P., CARPENTER M., *Cryst. Growth Des.*, 11 (2011) 1091.
[9] WENCKA M., VRTNIK S., JAGODIC M., JAGLICIC Z., TURCZYNSKI S., PAWLAK D. A., DOLINSEK J., *Phys. Rev. B*, 80 (2009), 24410.
[10] PAWLAK D.A., ŁUKASIEWICZ T., CARPENTER M., MALINOWSKI M., DIDUSZKO R., KISIELEWSKI J., *J. Cryst. Growth*, 282 (1 – 2), (2005) 260.
[11] KRUCZEK M., TALIK E., PAWLAK D.A., ŁUKASIEWICZ T., *Opt. Appl.*, 35 (3) (2005), 347.
[12] NOVOSELOV A., YOSHIKAWA A., SOLOVIEVA N., NIKL M., *Cryst. Res. Technol.*, 42 (2007), 132.
[13] NOGINOV M.A., LOUTTS G.B., *J. Opt. Soc. Am. B*, 16 (1999), 3.
[14] NOGINOV M.A., LOUTTS G.B., WARREN M., *J. Opt. Soc. Am. B*, 16 (1999), 475.
[15] YOON D.H., YONENAGA I., OHNISHI N., FUKUDA T., *J. Cryst. Growth*, 142 (1994) 339.
[16] YU Y.M., CHANI V.I., SHIMAMURA K., INABA K., FUKUDA T., *J. Cryst. Growth*, 177 (1997) 74.
[17] CHANI V.I., YOSHIKAWA A., MACHIDA H., FUKUDA T., *J. Cryst. Growth*, 212 (2000), 469.

[18] PAWLAK D.A., KAGAMITANI Y., YOSHIKAWA A., WOZNIAK K., SATO H., MACHIDA H., FUKUDA T., *J. Cryst. Growth*, 226 (2001), 341.
[19] WIERZBICKA E., KŁOS A., LEFELD-SOSNOWSKA M., PAJĄCZKOWSKA A., *Phys. Status Solidi A*, 203 (2006), 220.
[20] ESPINOZA G., *J. Chem. Phys.*, 37 (1962), 2344.
[21] BARAN M., ZHYDACHEVSKII Y., SUCHOCKI A., RESZKA A., WARCHOL S., DIDUSZKO R., PAJĄCZKOWSKA A., *Opt. Mater.*, 34 (2012), 604.
[22] MOULDER J., STICKLE W., SOBOL P., BOMBEN K., *Handbook of X-ray Photoelectron Spectroscopy*, Physical Electronics, Minnesota, 1995.
[23] OGASAWARA H., KOTANI A., POTZE R., SAWATZKY G.A., HOLE B.T., *Phys. Rev. B*, 44 (1991), 5465.
[24] BIANCONI A., KOTANI A., OKADA K., GIORGI R., GARGANO A., MARCELLI A., MIYAHARA T., *Phys. Rev. B*, 38 (1998), 3433.

Received 2014-05-25
Accepted 2014-08-21